LETTERS

Microscopic artificial swimmers

Rémi Dreyfus[1], Jean Baudry[1], Marcus L. Roper[2], Marc Fermigier[3], Howard A. Stone[2] & Jérôme Bibette[1]

Microorganisms such as bacteria and many eukaryotic cells propel themselves with hair-like structures known as flagella, which can exhibit a variety of structures and movement patterns[1]. For example, bacterial flagella are helically shaped[2] and driven at their bases by a reversible rotary engine[3], which rotates the attached flagellum to give a motion similar to that of a corkscrew. In contrast, eukaryotic cells use flagella that resemble elastic rods[4] and exhibit a beating motion: internally generated stresses give rise to a series of bends that propagate towards the tip[5–7]. In contrast to this variety of swimming strategies encountered in nature, a controlled swimming motion of artificial micrometre-sized structures has not yet been realized. Here we show that a linear chain of colloidal magnetic particles linked by DNA and attached to a red blood cell can act as a flexible artificial flagellum. The filament aligns with an external uniform magnetic field and is readily actuated by oscillating a transverse field. We find that the actuation induces a beating pattern that propels the structure, and that the external fields can be adjusted to control the velocity and the direction of motion.

To achieve controlled motion or swimming of manmade microstructures, two conditions need to be fulfilled. First, energy should be injected and transferred into a mechanical deformation of the device. Second, the sequence of deformations must be cyclic and not time-reversible. The second requirement arises from the fact that fluid dynamics at the micrometre scale is dominated by viscous rather than inertial terms. This means that a purely reversible internal displacement is not associated with any net motion (the 'scallop theorem')[8], and that a propelled microscopic device must thus use a swimming strategy that breaks the time-reversal invariance[8–10]. In the case of spermatozoa, for example, a bending wave propagates from the head towards the tail, inducing a net translational velocity. The issue of the direction of this motion is related to the structure of the filament. More precisely, the filament surface governs the ratio of the tangential viscous coefficient $\zeta_{\parallel}$ to the perpendicular viscous coefficient $\zeta_{\perp}$ (refs 6, 7). For smooth flagella, slender-body theory[11] gives $\zeta_{\perp}/\zeta_{\parallel} \approx 2$, so that the wave and overall velocity have opposite directions. By contrast, for flagella decorated with mastigonemes (hair-like filaments), the effective tangential resistive coefficient becomes much larger than the effective perpendicular resistive coefficient[12], so that flagella carrying mastigonemes swim in the same direction as the propagating wave. The propulsion exerted by microorganisms has motivated some theoretical and numerical modelling[6,9,13], especially for natural flexible filaments[14,15]. For this kind of swimmer, one relevant dimensionless parameter, previously called the 'sperm number'[16], is shown to be:

$$S_p = L/\left(\frac{\kappa}{\zeta_{\perp}\omega}\right)^{1/4}$$

where L is the length of the filament, κ the bending rigidity, and ω the angular frequency of the driving. S_p represents the relative importance of viscous to elastic stresses on the filament. For the so-called 'one-armed swimmer' two regimes were predicted: one dominated by internal elasticity at low S_p and the other dominated by viscous friction at high S_p. Between these two regimes, the existence of a maximum normalized swimming speed $V/L\omega$ was predicted for S_p of the order of unity. At this time, spermatozoa provide the only available experimental data and, using current experimental estimates of their stiffness[16], seem to operate at $S_p = 7$. Motivated by these two regimes and their potential involvement in the propulsion mechanism of real flagella, we attempt to measure the swimming velocity of a controlled manmade swimmer as a function of the dimensionless number S_p and ask whether there is indeed a maximum and how it depends on the type of actuation.

Our microscopic device consists of two parts: a magnetically activated 'flagellum' that provides propulsion, and a second part, which is the object to be transported (a red blood cell is the example shown here). The flagellum is made of micrometre-scale magnetic colloids attached together by short flexible joints. The filament is driven by a time-varying magnetic field that transfers energy and leads to motion. Indeed, the filament tends to follow the field direction, and so by oscillating the orientation of the net magnetic field we actuate the filament. However, as a consequence of its flexibility and viscous friction, reorientation is also associated with bending. The coupling between magnetic forces, filament flexibility and the viscous drag from the solvent that acts on the filament generates controlled deformations. With the proper field conditions and flexibility, the time-reversal invariance of the filament deformations is broken, and thus the attached cell is propelled.

The filaments are made of superparamagnetic 1-μm-diameter colloids linked[17,18] by several 107-nm-long (315 base pairs, bp) double-stranded DNAs as sketched in Fig. 1. The length and number of the DNA linkers and the particle diameter control the flexibility. These filaments are attached by one end to a red blood cell following the sample preparation procedure described in the 'Sample preparation' section of the Methods. To generate motion in a controlled direction and with a controlled speed, two magnetic fields are used. A

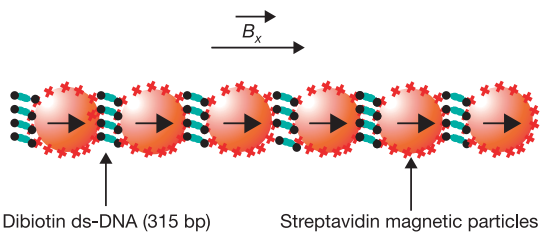

Figure 1 | Schematic representation of a flexible magnetic filament. The magnetic particles are coated with streptavidin (red cross symbols). Under an applied magnetic field B_x the particles form filaments. Double-stranded DNA with biotin at each end can bind the particles together via the specific biotin–streptavidin interaction. The experiments are performed with 8.4×10^4 DNAs per particle.

[1]Laboratoire Colloïdes et Matériaux Divisés, ESPCI, UMR CNRS 7612 UPMC, ParisTech, 10 rue Vauquelin, 75005 Paris, France. [2]Division of Engineering and Applied Sciences, Harvard University, Cambridge, Massachusetts 02138, USA. [3]Laboratoire Physique et Mécanique des Milieux Hétérogènes, ESPCI, UMR CNRS 7636, ParisTech, 10 rue Vauquelin, 75005 Paris, France.

© 2005 Nature Publishing Group

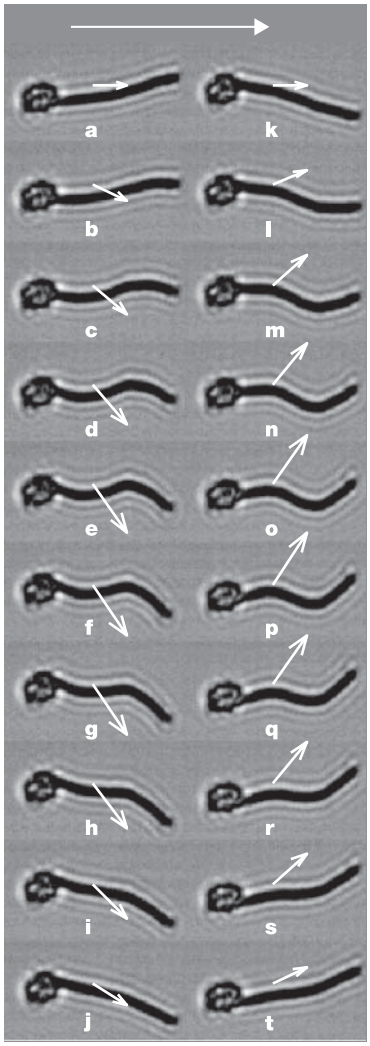

Figure 2 | Beating pattern of the motion of a magnetic flexible filament attached to a red blood cell. The time interval between each image is 5 ms. The white arrows represent the magnetic field ($B_x = 8.3$ mT, $B_y = 13.7$ mT, $f = 10$ Hz). The white arrow on the top shows the direction of motion. The filament length is $L = 24\,\mu$m.

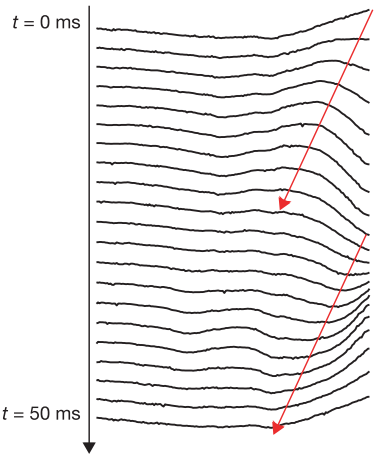

Figure 3 | Sequence of deformation of the end of a free filament. The propagation of a bending wave is indicated by the arrows. Conditions for the magnetic field: $B_x = 9$ mT, $B_y = 14$ mT, $f = 20$ Hz. Each image corresponds to pictures taken every 2.5 ms. The length of the portion of the filament shown is 34 μm.

homogeneous static field $\mathbf{B}_x = B_x\mathbf{x}$ imposes a straight configuration to the filament. In addition, a sinusoidal field $\mathbf{B}_y = B_y\sin(2\pi ft)\mathbf{y}$ with an adjustable frequency f is applied in the direction perpendicular to $\mathbf{B}_x$. These two fields have comparable amplitude so that the resulting field $\mathbf{B}_e$ oscillates around the x axis.

Because the particles are superparamagnetic, they acquire a magnetic dipole when subjected to a magnetic field. As the beads are known to have a preferred magnetization direction[19], there are two different contributions to the magnetic torque exerted upon the filament: the first contribution is due to the dipolar interactions between the beads, and the second contribution is due to the interaction between the dipole and the external field. Both effects cause the filament to pivot to follow the magnetic field. We use a fast camera to record the dynamics of a microstructure formed by a red blood cell specifically bound to one end of a 30-μm-long filament. As the transverse field $\mathbf{B}_y$ oscillates, the free end of the filament successively bends to follow the resulting field, which creates an undulation that propagates towards the attachment point.

In Fig. 2a–t we show a sequence of pictures of the dynamics during one period. The wave propagation, which is responsible for the non-reversible displacements of the filament, is visible in Fig. 3 in which we have superimposed the skeleton of each profile. We find that the overall displacement of this swimmer is always directed towards the free extremity of the filament (see the Supplementary Movies) and opposite to the propagation of the bending wave[7]. This behaviour is an intrinsic consequence of these magnetically actuated flagella. The bending wave propagates from the free end because it is the most mobile and has the largest-amplitude displacement although the entire filament is magnetically actuated. By contrast, spermatozoa for which the bending wave propagates from head to tail move in the direction of the head. The 'roughness' of the filament evidently has no decisive impact upon the swimming direction, which, just as for smooth flagellum, opposes the direction of bending-wave propagation. This is in agreement with previous experiments and simulations[20,21] that prove that a chain of spheres has almost the same drag coefficient as a prolate spheroid of the same length and aspect ratio. The mean swimming velocity of this device is always found collinear to the static field $\mathbf{B}_x$ and has a maximum of about the diameter of a red blood cell per second. As a final remark, we note that within the same sample we have sometimes observed two different swimming devices moving in opposite directions according to their initial orientation, which rules out any suspected consequences of residual field gradients. The Supplementary Movies show the dynamics of the filament at two frame rates: 440 frames s^{-1} (Supplementary Movie 1) and 40 frames s^{-1} (Supplementary Movie 2), for which $L = 12\,\mu$m, $f = 10$ Hz, $B_x = 9$ mT, $B_y = 14.5$ mT.

The physics of the motion of the magnetic filament can be described by the equations briefly presented in the 'Equation of motion' section of the Methods and detailed in the Supplementary Information. The final equations of motion involve three dimensionless numbers: S_p as previously defined, $b_0 = B_y/B_x$, and the magneto-elastic number:

$$M_n = \frac{2\pi(aB_xL)^2}{3\mu_0\kappa}\left(\frac{\chi_{\parallel} - \chi_{\perp} + \chi_{\parallel}\chi_{\perp}/4}{(1-\chi_{\parallel}/6)(1+\chi_{\perp}/12)}\right)$$

where $\chi_{\parallel}$ is the susceptibility of the easy direction, $\chi_{\perp}$ the susceptibility in the orthogonal direction, a the radius of the particles, and μ_0 the magnetic permeability in free space. To measure κ and estimate M_n, we assume the susceptibilities ($\chi_{\parallel}$ and $\chi_{\perp}$) to be identical and equal to the value given by the manufacturer (see 'Parameters measurement' section in the Methods).

In Fig. 4, we plot the measured scaled swimming velocity $V/L\omega$ as a function of S_p, for three different values of M_n. As predicted[14,15], the normalized velocity has a maximum; however, it is clear that its

© 2005 Nature Publishing Group

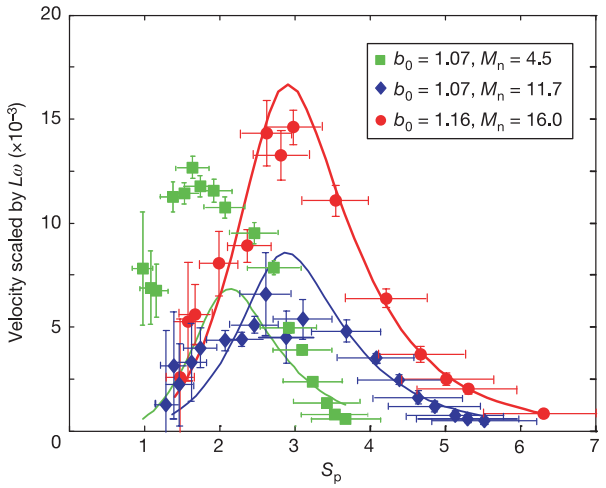

Figure 4 | Scaled velocity as a function of S_p. Experimental data are discrete points while the continuous lines are the predictions obtained with our model. Error bars for the scaled velocity are estimated by measuring the drift velocity of a filament when $B_y = 0$ and error bars for S_p correpond to the standard deviation of S_p calculated by estimating the standard deviation of κ. The cell radius a_s and the distance a_l of the attachment point from the cell centre are evaluated from experimental images. Green squares: $\kappa = 3.3 \times 10^{-22}\,\mathrm{J\,m^{-1}}$, $L = 13\,\mu\mathrm{m}$, $B_x = 8.7\,\mathrm{mT}$, $B_y = 9.3\,\mathrm{mT}$, $a_s = 3.2\,\mu\mathrm{m}$, $a_l = 3.2\,\mu\mathrm{m}$. Blue diamonds: $\kappa = 3.3 \times 10^{-22}\,\mathrm{J\,m^{-1}}$, $L = 21\,\mu\mathrm{m}$, $B_x = 8.7\,\mathrm{mT}$, $B_y = 9.3\,\mathrm{mT}$, $a_s = 2.7\,\mu\mathrm{m}$, $a_l = 0\,\mu\mathrm{m}$. Red circles: $\kappa = 3.3 \times 10^{-22}\,\mathrm{J\,m^{-1}}$, $L = 24\,\mu\mathrm{m}$, $B_x = 8.9\,\mathrm{mT}$, $B_y = 10.3\,\mathrm{mT}$, $a_s = 3.1\,\mu\mathrm{m}$, $a_l = 3.1\,\mu\mathrm{m}$.

position depends on the field strength since it shifts from $S_p = 1.8$ to 2.8 when the dimensionless field strength M_n varies from 3.4 to 10.3. The maximum normalized velocity corresponds for each value of the magnetoelastic number to the optimal balance between elasticity, magnetically induced internal forces and viscous forces.

In our experimental realization of a controllable swimming microdevice, a magnetically actuated flexible filament has the ability to exhibit, in a precise regime, a non-reciprocal motion responsible for propulsion. The internal torques, originating from a combination of dipolar colloidal interactions and anisotropy of the susceptibility, can be externally controlled so that the velocity and the direction of motion can be chosen. This swimming device displays a maximum normalized velocity as a function of the dimensionless parameter S_p, as already predicted in the case of model elastic filaments. However, in our device this optimal combination is shown to depend also on a distinct parameter, M_n, that involves the actuating field strength. We hope that a deeper understanding of this effect may clarify the consequences of actuation type and mechanism on the optimal conditions for swimming in nature. These magnetically actuated colloidal devices might possibly also be useful in the precise and selective positioning of micro-objects or the controlled motion of minute quantities of surrounding fluids[22,23].

METHODS

Sample preparation. Biotinylated double-stranded DNAs (315 bp) are synthesized using the polymerase chain reaction (PCR) kit (Expand High Fidelity PCR System) provided by Roche Applied Science using biotinylated primers (Eurogentec) and a λ-DNA template. The resulting DNA solution is purified and its concentration is measured by fluorescence (Picogreen).

Human red blood cells (6 μl) are first washed three times in 500 μl PBS buffer. Then, they are incubated for 30 min in 1 ml of Biotinylated PEG-NHS (3,400 Da) provided by Nektar Therapeutics in a PBS buffer. After 1 min the sample is centrifuged at 400*g*. and the cells are redispersed in 500 μl of PBS buffer containing a pluronic surfactant (F-127) at 0.5% by weight.

Superparamagnetic particles of 1 μm in diameter ($\sim 10 \times 10^9$ beads $\mathrm{ml^{-1}}$) provided by Dynal (Dynabeads MyOne Streptavidin) with streptavidin grafted onto their surface (7×10^5 streptavidin molecules per particle) are diluted 10× in a PBS buffer with F-127 (0.5 wt%). They are washed twice following this procedure before storing them in this buffer. In a 1,000-μl Eppendorf tube we mix: 0.5 μl of 315-bp DNA (1.4×10^{-6} M), 40 μL of PBS buffer containing 0.5 wt% of F-127, 5 μl of the 10 × diluted streptavidin beads, and 10 μl of the biotinylated red blood cells solution. The Eppendorf tube is placed in a spatially homogeneous magnetic field (30 mT) for 15 min. 10 μl of the solution is then added to 40 μL of PBS buffer with F-127 (0.5 wt%). These assemblies are transferred into a capillary (2 cm × 100 μm × 1 mm) that is sealed at both extremities with highly viscous silicone oil (Rhodia). Because this last step can be responsible for the breaking of the structures, we recover them by replacing the capillary in the same magnetic field (30 mT) for 5 min.

Equation of motion. In the Supplementary Information, we derive equations of motion for the filament, which is modelled as a magnetically driven inextensible elastic rod. An expression for the torque resultant upon the filament is given that incorporates both dipole–dipole interactions between the beads in the chain and possible anisotropy in the magnetic susceptibility of the beads. The filament swims close to the floor of the capillary tube, and therefore experiences greatly enhanced drag. The red blood cell is approximately disk-shaped; we determine its radius a_s from the video images, and assume that it has the same approximate thickness (which sets the distance from the filament to the tube floor, h). The red blood cell sits on a thin film of fluid of thickness d, where d is used as a fitting parameter to ensure agreement at high frequency. d is set physically by a combination of steric and electrostatic interactions between the red blood cell glycocalyx and the coating on the capillary tube floor, and by elastohydrodynamic lift forces generated by the moving red blood cell. We suppose that the former effect is dominant, so that d is independent of swimming speed for a given swimmer. The torque and stress resultants vanish at the free end of the filament. At the tethered end, the moment and force are balanced against the rotational and viscous drags upon the red blood cell, which are dominated by the contribution from the lubrication layer.

Parameters measurement. The bending rigidity κ of the filament is measured from the hairpin shape as previously described[17], by using the formula $C_{\max} = \sqrt{\frac{\pi}{3}\frac{B}{2a}}\sqrt{\frac{a^4\chi^2}{\kappa\mu_0}}$, where $C_{\max}$ is the maximum of curvature and χ is the magnetic susceptibility, which is slightly dependent on B and which is given by the manufacturer ($\chi \approx 1$). We find $\kappa = (3.3 \pm 1.6) \times 10^{-22}\,\mathrm{J\,m^{-1}}$. This value is comparable to the one found for real flagella[24,25]: $\kappa = 4 \times 10^{-22}\,\mathrm{J\,m^{-1}}$. We took $\zeta_\perp = 4\pi\eta$ (refs 15, 24 and 26).

Received 25 March; accepted 29 July 2005.

1. Bray, D. *Cell Movements: from Molecules to Motility* 6–12 (Garland Publ., New York, 1992).
2. Berg, H. C. & Anderson, R. A. Bacteria swim by rotating their flagellar filaments. *Nature* **245**, 380–384 (1973).
3. Schuster, S. C. & Khan, S. The bacterial flagellar motor. *Annu. Rev. Biophys. Biomol. Struct.* **23**, 509–539 (1994).
4. Gibbons, I. R. Cilia and flagella of eukaryotes. *J. Cell Biol.* **91**, S107–S124 (1981).
5. Satir, P. Studies on cilia. 3. Further studies on cilium tip and a sliding filament model of ciliary motility. *J. Cell Biol.* **39**, 77–94 (1968).
6. Taylor, G. I. Analysis of the swimming of microscopic organisms. *Proc. R. Soc. Lond. Ser. A* **209**, 447–461 (1951).
7. Gray, J. & Hancock, G. J. The propulsion of sea-urchin spermatozoa. *J. Exp. Biol.* **32**, 802–814 (1955).
8. Purcell, E. M. Life at low Reynolds number. *Am. J. Phys.* **45**, 3–11 (1977).
9. Becker, L. E., Koehler, S. A. & Stone, H. A. On self-propulsion of micro-machines at low Reynolds number: Purcell's three-link swimmer. *J. Fluid Mech.* **490**, 15–35 (2003).
10. Najafi, A. & Golestanian, R. Simple swimmer at low Reynolds number: Three linked spheres. *Phys. Rev. E.* **69**, 062901–062904 (2004).
11. Cox, R. G. Motion of long slender bodies in a viscous fluid. Part I. General theory. *J. Fluid Mech.* **45**, 791–810 (1971).
12. Brennen, C. Locomotion of flagellates with mastigonemes. *J. Mechanochem. Cell Motil.* **3**, 207–217 (1976).
13. Avron, J. E., Gat, O. & Kenneth, O. Optimal swimming at low Reynolds numbers. *Phys. Rev. Lett.* **93**, 186001–186004 (2004).
14. Lagomarsino, M. C., Capuani, F. & Lowe, C. P. A simulation study of the dynamics of a driven filament in an Aristotelian fluid. *J. Theor. Biol.* **224**, 215–224 (2003).
15. Wiggins, C. H. & Goldstein, R. E. Flexive and propulsive dynamics of elastica at low Reynolds number. *Phys. Rev. Lett.* **80**, 3879–3882 (1998).
16. Lowe, C. P. Dynamics of filaments: modelling the dynamics of driven microfilaments. *Phil. Trans. R. Soc. Lond. B* **358**, 1543–1550 (2003).
17. Goubault, C. *et al.* Flexible magnetic filaments as micromechanical sensors. *Phys. Rev. Lett.* **91**, 260802–260805 (2003).
18. Koenig, A. *et al.* Magnetic force probe for nanoscale biomolecules. *Phys. Rev. Lett.* (in the press).

© 2005 Nature Publishing Group

19. Strick, T. R., Allemand, J. F., Bensimon, D., Bensimon, A. & Croquette, V. The elasticity of a single supercoiled DNA molecule. *Science* **271,** 1835–1837 (1996).
20. Zahn, K., Lenke, R. & Maret, G. Friction coefficient of rod-like chains of spheres at very-low Reynolds-numbers.1. Experiment. *J. Phys. II* **4,** 555–560 (1994).
21. Meunier, A. Friction coefficient of rod-like chains of spheres at very-low Reynolds-numbers.2. Numerical simulations. *J. Phys. II* **4,** 561–566 (1994).
22. Terray, A., Oakey, J. & Marr, D. W. M. Microfluidic control using colloidal devices. *Science* **296,** 1841–1844 (2002).
23. Darnton, N., Turner, L., Breuer, K. & Berg, H. C. Moving fluid with bacterial carpets. *Biophys. J.* **86,** 1863–1870 (2004).
24. Camalet, S., Julicher, F. & Prost, J. Self-organized beating and swimming of internally driven filaments. *Phys. Rev. Lett.* **82,** 1590–1593 (1999).
25. Ishijima, S. & Hiramoto, Y. Flexural rigidity of echinoderm sperm flagella. *Cell Struct. Funct.* **19,** 349–362 (1994).
26. Wiggins, C. H., Riveline, D., Ott, A. & Goldstein, R. E. Trapping and wiggling: Elastohydrodynamics of driven microfilaments. *Biophys. J.* **74,** 1043–1060 (1998).

Supplementary Information is linked to the online version of the paper at www.nature.com/nature.

Acknowledgements We thank the Imphy Company for providing us with free Mumetal. We also thank A. Ajdari, J. Prost, J.-B. Salmon and D. Weitz for discussions, and C. Gosse, A. Koenig, F. Montel and C. Goubault for help in material preparation.

Author Information Reprints and permissions information is available at npg.nature.com/reprintsandpermissions. The authors declare no competing financial interests. Correspondence and requests for materials should be addressed to R.D. (remi.dreyfus@espci.fr).

© 2005 Nature Publishing Group